Strain-rate dependent shear viscosity of the Gaussian core model fluid

Alauddin Ahmed,[1] Peter Mausbach,[2] and Richard J. Sadus[1,a)]
[1]*Centre for Molecular Simulation, Swinburne University of Technology, P.O. Box 218, Hawthorn, Victoria 3122, Australia*
[2]*Cologne University of Applied Sciences, 50679 Cologne, Germany*

(Received 13 August 2009; accepted 19 November 2009; published online 10 December 2009)

Nonequilibrium molecular dynamics simulations are reported for the shear viscosity of the Gaussian core model (GCM) fluid over a wide range of densities, temperatures and strain rates. A transition from Newtonian and non-Newtonian behavior is observed in all cases for sufficiently high strain rates. On the high-density side of the solid region where re-entrant melting occurs, the shear viscosity decreases significantly when the density is increased at constant temperature and Newtonian behavior persists until very high strain rates. This behavior, which is attributed to particle overlap, is in contrast to the monotonic increase in shear viscosity with density observed for the Lennard-Jones potential. Contrary to the behavior of normal fluids, the viscosity is observed to increase with increasing temperatures at high densities. This reflects a peculiarity of the GCM, namely the approach to the "infinite-density ideal-gas limit." The behavior is also consistent with viscosity measurements of cationic surfactant solutions. In contrast to other potentials, the shear viscosities for the Gaussian core potential at low to moderate strain rates are obtained with modest statistical uncertainties. Zero shear viscosities extrapolated from the nonequilibrium simulations are in good agreement with equilibrium Green–Kubo calculations. © *2009 American Institute of Physics*. [doi:10.1063/1.3273083]

I. INTRODUCTION

The viscoelastic behavior of nonequilibrium fluids is of significant theoretical and industrial interest.[1,2] It has been experimentally determined that many fluids display shear thinning, which is characterized by a decrease in viscosity with increasing strain rate.[2] In contrast, some complex fluids, such as colloidal suspensions show shear thickening, i.e., their shear viscosities increase with increasing strain rate.[2] Theoretical studies of flows under shear have largely focused on unbounded interaction potentials, such as hard spheres or the Lennard-Jones potential.[3] However, during the past decade bounded potentials such as the Gaussian core model (GCM) have proved useful in the field of soft condensed matter physics.[4]

Recent studies,[5,6] indicate that the equilibrium transport properties of the GCM fluid show anomalous behavior at some state points. The self-diffusion coefficient and shear viscosity were obtained from equilibrium molecular dynamics using the Green–Kubo formulae. At constant temperature but increasing density, the diffusivity increased and the shear viscosity decreased, violating the Stokes–Einstein relation.[7] An interesting relationship between equilibrium transport anomalies and the excess entropy for a Gaussian core (GC) system was recently discussed elsewhere.[6,8] Anomalous thermodynamics and the microscopic structure for a different core-softened fluid involving a combination of the Lennard-Jones potential and a Gaussian well were also studied recently.[9] The occurrence of equilibrium transport anomalies in the GCM fluid gives rise to the question of whether or not the strain rate dependent shear viscosity is also anomalous.

In a number of studies the GCM is used as an *effective* potential to explain aspects of soft condensed matter. For example, the effective interaction between self-avoiding polymer coils, dispersed in a good solvent, can be described by the GCM.[10,11] Additionally, the GCM has been applied[12] to micelle aggregates to reproduce results from calorimetric experiments of aqueous suspension of the ionic surfactant sodium. Simulation of such aggregates built up from several thousands of molecules become rapidly intractable if a detailed description on an atomic level is retained. It is therefore tempting to consider such aggregates as "soft" particles where the detailed interaction is replaced by an effective interaction between the soft particles.

The aim of our study is to contribute to the understanding of flow phenomena under shear for fluid particles with bounded soft potentials. We report nonequilibrium molecular dynamics[13] (NEMD) calculations for the shear viscosity behavior of GCM fluids at different strain rates and state points. To the best of our knowledge no nonequilibrium studies have been reported using potentials, such as the GCM, which permits particle overlap.

II. THEORY

A. Intermolecular potential

We studied a system of particles without structure, interacting via the GC potential

a)Electronic mail: rsadus@swin.edu.au.

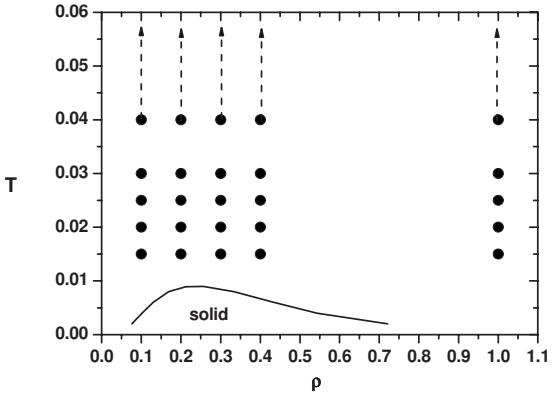

FIG. 1. Phase diagram of the GCM fluid showing the state points (●) covered by the NEMD simulations reported in this work.

$$u(r) = \varepsilon \exp\left[-\left(\frac{r}{\sigma}\right)^2\right], \tag{1}$$

where ε and σ are the height and width of the potential. A feature of Eq. (1) is that the particles can overlap, i.e., $r \leq \sigma$, without catastrophic consequences for the simulation.

B. Simulation details

The initial configuration in all the simulations was a face centered cubic lattice structure. The isothermal isochoric NEMD simulations were performed by applying the standard *sllod* equations[13] of motion for planar Couette flow coupled with Lees–Edwards[13,14] periodic boundary conditions. A Gaussian thermostat multiplier[15] was used to keep the kinetic temperature of the fluid constant. The equations of motion were integrated with a five-value Gear predictor-corrector scheme.[16,17] The normal conventions were used for the reduced density ($\rho^* = \rho\sigma^3$), temperature ($T^* = kT/\varepsilon$), energy ($E^* = E/\varepsilon$), pressure ($p^* = p\sigma^3/\varepsilon$), viscosity ($\eta^* = \eta\sigma^2/\sqrt{m\varepsilon}$), strain rate ($\dot{\gamma}^* = \dot{\gamma}\sqrt{m\sigma^2/\varepsilon}$), and time ($\tau^* = \tau\sqrt{\varepsilon/m\sigma^2}$). All quantities quoted in this work are in terms of these reduced quantities and the asterisk superscript will be omitted in the rest of the paper.

The simulations covered five isochors of densities $\rho = 0.1$, 0.2, 0.3, 0.4, and 1.0, temperatures ranging from $T = 0.015$ to 3.0 and various strain rates from $\dot{\gamma} = 0.005$ to 9.0. The phase state points for our NEMD simulations are shown in Fig. 1. The solid-liquid coexisting lines in Fig. 1 are calculated using the GWTS-algorithm.[14,18] Since our simulations covered a wide range of temperatures and densities we had to carefully choose the integration time step for different state points such that the time step was small enough to solve the equations of motion correctly and large enough to sample phase space adequately. The equations of motion were integrated with a time step of $\tau = 0.001$. The cutoff radius for the potential was 3.2σ. The ensemble averages are reported without any long-range corrections because the potential rapidly goes to zero at larger separations.

For each state point $(\rho, T, \dot{\gamma})$ simulation trajectories were typically run for 2×10^6 time steps. The first 4×10^5 time steps of each trajectory were used either to equilibrate zero-shearing field equilibrium molecular dynamics or to achieve nonequilibrium steady state after the shearing field was switched on. The remaining time steps in each trajectory were used to accumulate the average values of thermodynamic variables standard deviations. A system size of 4000 GC particles was used for all the simulations reported in this paper.

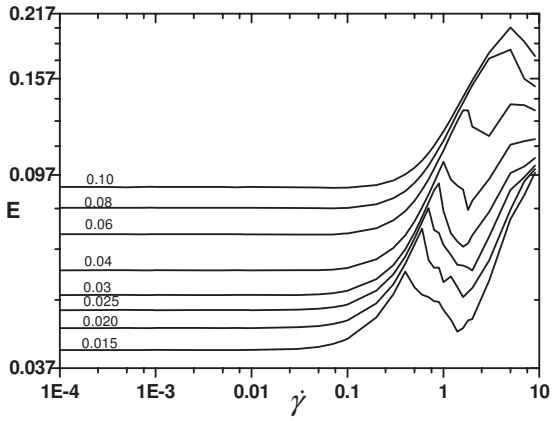

FIG. 2. Strain-rate dependent internal energy per particle as a function of strain rate for different constant temperatures (as indicated on the lines) at a density of $\rho = 0.1$. The sharp drop after the increase in energy indicates the occurrence of the string phase.

C. Maximum safe strain rates

A well-known limitation of the *sllod* algorithm coupled to a Gaussian thermostat is that it generates an artificial "string-phase" at high strain rates.[19–21] To avoid this problem and to also avoid possible shear-induced ordering effects in our analysis, we estimated the maximum strain rate that could be safely used by analyzing the strain-rate dependent internal energy per particle. The formation of strings of particles or shear-induced ordering causes a clear and easily detectable breakdown in the internal energy profiles. For example, in Fig. 2 we show the strain-rate dependent internal energy per particle for different temperatures at a density of $\rho = 0.1$. A similar trend can be observed using viscosity data, but the drop in the viscosity profiles is less pronounced, especially at higher strain rates. Using this procedure, we estimated the maximum safe strain rates at different densities and temperatures. These data are summarized in Table I.

We note that an alternative method for the accurate detection of string phases would be to observe the drop in the strain-rate configurational temperature.[22] There are also alternatives[23] to the use of a Gaussian thermostat which avoid the formation of the artificial string phases. Nonetheless, we found that the energy-drop method was sufficiently reliable to avoid string phases and no string phases were detected within the safe range of strain rates reported here.

III. RESULTS AND DISCUSSION

A. Shear viscosity: Strain-rate behavior

The shear viscosity as a function of strain rate at different temperatures and densities is illustrated in Fig. 3. In all cases we can observe a transition from Newtonian (strain-rate independent) to non-Newtonian (strain-rate dependent) behavior. For a given temperature up to densities of $\rho = 0.3$,

TABLE I. Maximum safe strain rates at different densities and temperatures. These strain rates avoid string phases and shear-induced ordering. For state points without an entry the drop in the internal energy profiles occurs at strain rates higher than a dimensionless value of 9.0. This situation occurs for all densities with temperatures greater than $T=0.30$.

T	$\rho=0.1$	$\rho=0.2$	$\rho=0.3$	$\rho=0.4$	$\rho=1.0$
0.015	0.4	0.4	0.5	1.2	3.0
0.020	0.6	0.8	1.2	1.8	3.0
0.025	0.7	1.0	1.6	2.0	5.0
0.030	0.9	1.2	2.0	3.0	5.0
0.040	1.0	1.8	3.0	5.0	7.0
0.060	1.6	5.0	5.0	7.0	⋯
0.080	3.0	7.0	7.0	⋯	⋯
0.100	5.0	⋯	⋯	⋯	⋯
0.300	⋯	⋯	⋯	⋯	⋯

the onset of this transition generally occurs at a lower strain rate as the density is increased. Similarly, for any given density, increasing the temperature also generally reduces the strain rate required to observe the transition between Newtonian and non-Newtonian behavior. The effect of temperature is somewhat weaker than the effect of density.

The above description is consistent with the behavior reported for the Lennard-Jones fluid. However, there is a very noticeable exception. Normally, we would expect the shear viscosity isochors (i.e., shear viscosity at constant density) to be progressively shifted to higher viscosity values, with increasing densities. At $T=0.015$ [Fig. 3(a)], the $\rho=0.1$, 0.2, and 0.3 isochors occur at progressively higher shear viscosities. This trend is arrested at the $\rho=0.4$ isochor, which straddles the $\rho=0.3$ isochor. The $\rho=1.0$ isochor commences at viscosities less than that observed for $\rho=0.2$. Furthermore, the onset of non-Newtonian behavior does not occur until much higher strain rates. The non-Newtonian part of these anomalous isochors occurs in the conventional density sequence relative to the non-Newtonian parts of the other isochors. Very high strain rates appear to restore normal behavior in the non-Newtonian region. Increasing the temperature to $T=0.020$ [Fig. 3(b)], 0.025 [Fig. 3(c)] progressively removes the anomalous behavior at all strain rates. The crossover point to normal behavior is at a temperature of $T=0.030$ [Fig. 3(d)]. We performed additional calculations for temperatures up to $T=1.0$. At these higher temperatures (Fig. 4), normal behavior was observed.

This anomalous behavior reflects an approaching solid state transition at low temperatures and moderately high densities (around $\rho\approx0.25$) at which the shear viscosity rises sharply [see Fig. 4a in Ref. 6]. Re-entrant melting occurs on the high-density side of the solid region (Fig. 1), which again results in a decrease in the shear viscosity for densities near the melting density.

Anomalous shear behavior $(\partial\eta_0/\partial\rho)_T<0$ has also been reported[6] in equilibrium calculations at temperatures up to approximately $T=0.032$, which coincides with the anomalous range of temperature observed here. In this region the slope of the density dependent viscosity along an isotherm can be characterized within three different stages [see Fig. 4b in Ref. 6]. For $\rho\leq0.3$, the zero-shear viscosity increases with increasing the density, which is typical for "normal" liquids. Thereafter, the zero-shear viscosity passes through a maximum, followed by an anomalous decrease in η_0 upon further compression. At higher densities, the zero-shear viscosity passes through a minimum and increasing the density further at constant temperature again causes an increase in η_0. The last situation coincides with a region of very high particle overlap. For $T>0.032$, the anomaly disappears and η_0 increases with increasing ρ.

Figure 5 illustrates the viscosity profiles at $\rho=1.0$ for temperatures ranging from $T=0.04$ to 3 and strain rates starting from $\dot{\gamma}=0.005$. Generally, the viscosity increases with temperature, which is contrary to the behavior of normal dense liquids. However, at very high densities where penetration of GC particles is dominant and the repelling force between the particles becomes very small, the GCM system approaches the so called "infinite-density ideal-gas limit."[10] Many thermodynamic and dynamic quantities indicate[5] that the GCM system is approaching this limit at a density of $\rho=1.0$ and here, the system behaves like a dense gas rather than a dense liquid. The unusual temperature dependence of the viscosity shown in Fig. 5 reflects this peculiarity of the GCM and the viscosity behavior at this density is in excellent agreement with equilibrium Green–Kubo calculations.[6]

We note that there is recent experimental evidence[24] for such abnormal behavior. Kalur *et al.*[24] measured the viscosity behavior of cationic surfactant solutions and observed an increase in viscosity with increasing temperature as depicted in Fig. 5. They attributed the anomaly to wormlike micelles. It is unlikely that such phenomena could be predicted using a conventional unbounded potential, which suggests that the GCM might have a useful role in understanding this aspect of surfactant behavior. It is also evident from Fig. 5 that increasing the temperature causes an increase in the degree of shear thinning, i.e., the crossover between the Newtonian and the non-Newtonian regime is shifted to lower strain rates.

NEMD simulation studies commonly suffer from the weakness that the quoted statistical uncertainties become increasingly large in the zero-shear limit. This means that the results cannot be applied directly to real fluids, which typically experience strain rates much lower than used in simulations. Nonetheless, as evident from Figs. 3–5, reasonable statistical uncertainties are obtained from the GCM at mod-

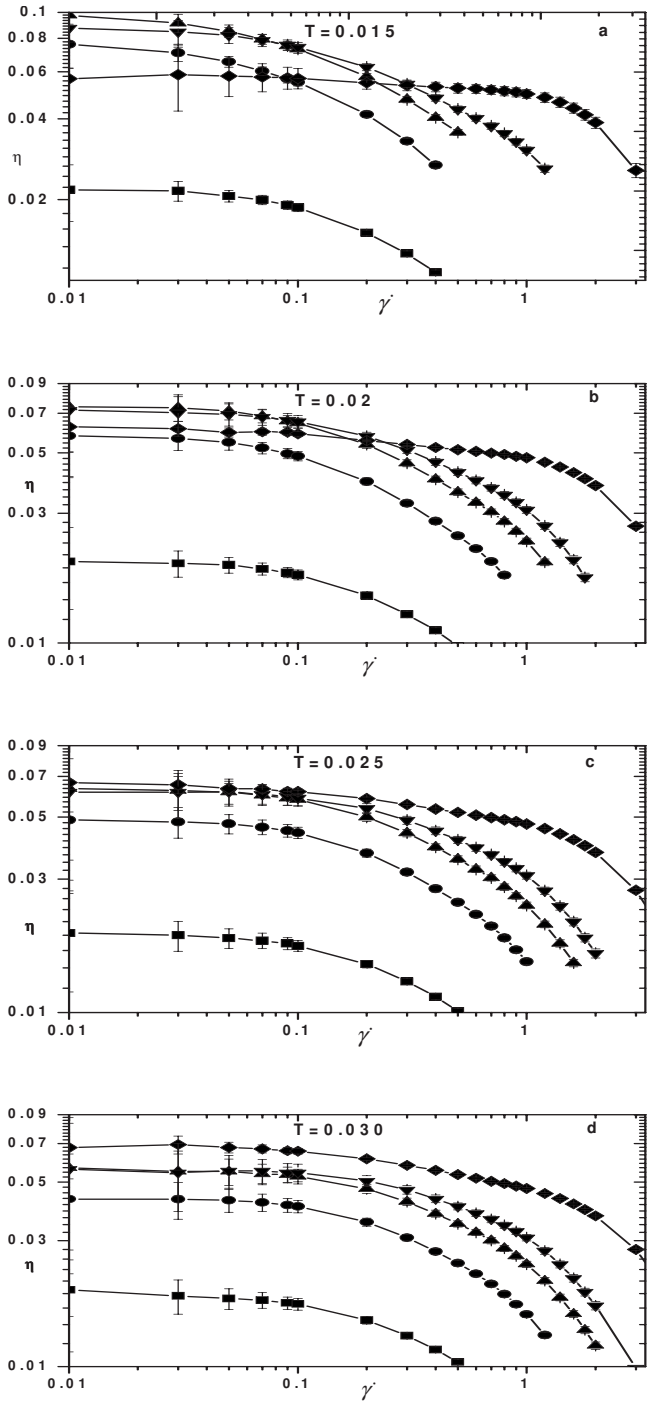

FIG. 3. Shear viscosity isochors as a function of strain rate for (a) $T=0.015$, (b) $T=0.02$, (c) $T=0.025$, and (d) $T=0.03$. The isochors were obtained for $\rho=0.1$ (■), 0.2 (●), 0.3 (▲), 0.4 (▼), and 1.0 (♦). Note the anomalous behavior at $\rho>0.3$. The lines are for guidance only.

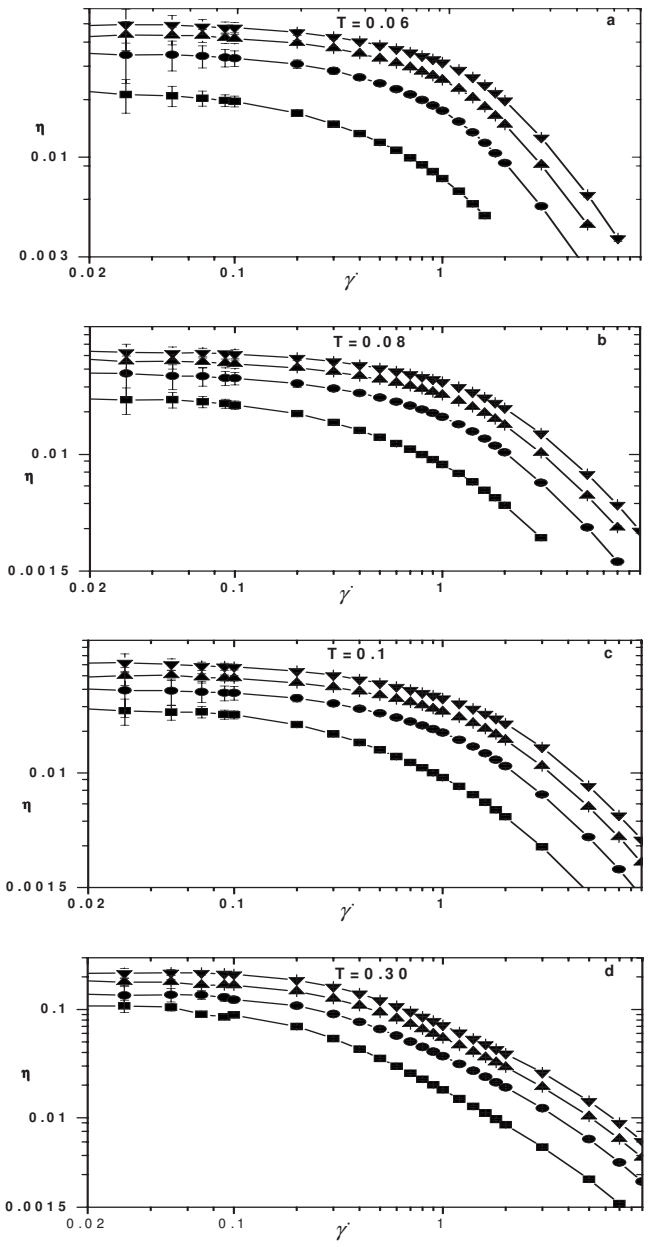

FIG. 4. Shear viscosity isochors as a function of strain rate for (a) $T=0.06$, (b) $T=0.08$, (c) $T=0.1$, and (d) $T=0.3$. The isochors were obtained for $\rho=0.1$ (■), 0.2 (●), 0.3 (▲), and 0.4 (▼). The lines are for guidance only.

erately low strain rates. The reliability of the calculations for low strain rates, improves with increasing density. The statistical uncertainties for the CGM are lower than observed for unbounded potentials such as the Lennard-Jones potential

B. Fitting simulation data

As discussed in detail elsewhere,[25–30] shear viscosity data can be fitted to relatively simple relationships such as

$$\eta = \eta_0 - \eta_1 \dot{\gamma}^{\alpha}, \tag{2}$$

where η_0 is the zero shear viscosity and η_1 is a coefficient, which depends on temperature and density. At temperatures at or near the triple point of a Lennard-Jones fluid, good agreement is obtained when $\alpha=\frac{1}{2}$, which is consistent with mode-coupling theory. However, better overall agreement[30] for other temperatures and densities can be obtained using other values of α. Figure 6 compares our simulation at $T=0.015$ and $\rho=0.01$, fitted to Eq. (2), using $\alpha=\frac{1}{2}$ ($\eta_0=0.0245$, $\eta_1=0.020$) and a best fit value of $\alpha=0.75$ ($\eta_0=0.0230$, $\eta_1=0.025$). It is evident from this comparison that using a value of $\frac{1}{2}$ fails to adequately reproduce the simulation data, particularly at moderate strain rates, whereas a value of $\alpha=0.75$ gives good agreement for the entire range

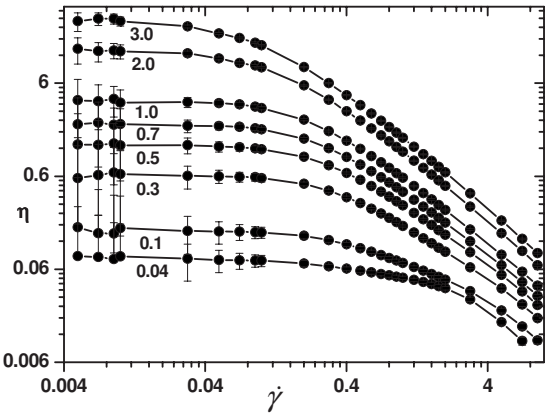

FIG. 5. Shear viscosity at $\rho=1.0$ vs strain rate for various temperatures as indicated. The lines are for guidance only.

of strain rates. The value of $\alpha=\frac{1}{2}$ is also an inadequate choice for other temperatures and densities (not shown).

C. Zero-shear viscosities

In view of the relatively modest statistical uncertainties reported at low to moderate strain rates, it is reasonable to extrapolate the NEMD results to zero strain rate and thereby obtain the equilibrium or zero-shear viscosities. It is of interest to compare these extrapolated values with equilibrium values obtained elsewhere[6] from Green–Kubo calculations. Figure 7 compares Green–Kubo and extrapolated NEMD zero-shear viscosities η_0 along isochors at $\rho=0.1$, 0.2, 0.3, 0.4, and 1.0 as a function of temperature. The comparison indicates that the discrepancies between NEMD zero shear viscosities than Green–Kubo calculations for $\rho\leq 0.4$ are typically less than 5%. For $\rho=1.0$, the NEMD values are between 1% and 12% higher than the Green–Kubo calculations. The zero-shear viscosity η_0 shows a nonmonotonic dependence on density for certain state conditions, which is consistent with equilibrium simulations.[6]

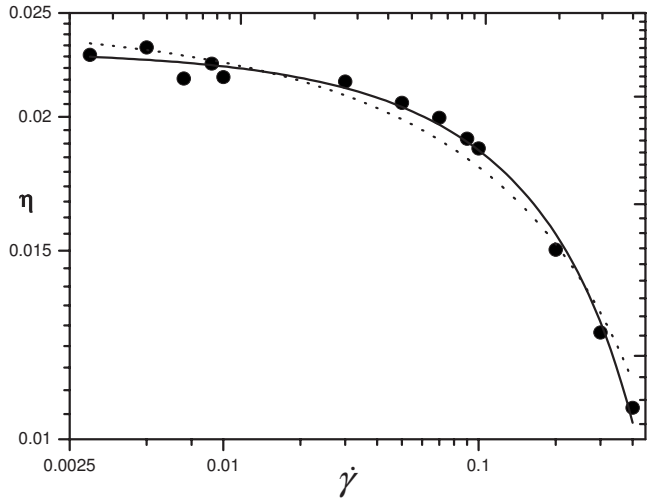

FIG. 6. Shear viscosity as a function of strain rate at $T=0.015$ and $\rho=0.01$. The lines indicate the fit to the simulation data (●) using Eq. (2) with $\alpha=\frac{1}{2}$ (dotted line) and 0.75 (solid line).

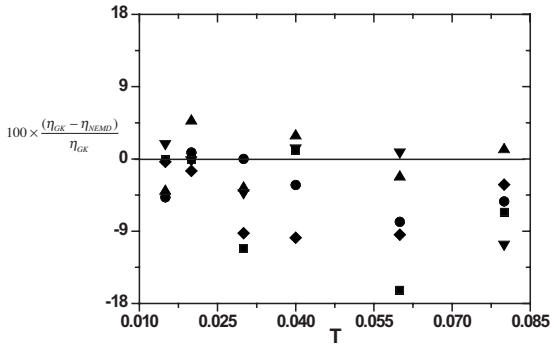

FIG. 7. Comparison of the relative percentage difference of zero-shear viscosities obtained from this work with Green–Kubo (GK) calculations (Ref. 6) as a function of temperature and densities of $\rho=0.1$ (■), 0.2 (●), 0.3 (▲), 0.4 (▼), and 1.0 (♦).

IV. CONCLUSIONS

NEMD simulations of the shear viscosity behavior of the GCM indicate anomalous behavior for shear viscosity isochors with respect to strain rate at low temperatures. The shear viscosity is lower than would be normally expected and the onset of shear thinning is delayed until much higher strain rates. The high strain rate, non-Newtonian region of the isochor appears to behave normally. Increasing the temperature progressively reduces the anomaly. At $T\geq 0.03$, the viscosity isochor behaves normally at all strain rates, which is consistent with zero-shear viscosity results for the GCM. The GCM viscosity increases with temperature at high densities, which is consistent with the behavior of dense gases when the GCM system is approaching the so called infinite-density ideal-gas limit. The statistical uncertainty in the viscosities reported for low strain rates is considerably less than can be obtained from the Lennard-Jones potential. Zero shear viscosities, extrapolated from the NEMD data, are in generally good agreement with equilibrium Green–Kubo calculations.

ACKNOWLEDGMENTS

Financial support from the Deutsche Forschungsgemeinschaft (DFG) is gratefully acknowledged. One of us (A.A.) thanks Swinburne University of Technology for a postgraduate scholarship.

[1] A. Onuki, J. Phys.: Condens. Matter **9**, 6119 (1997).
[2] H. A. Barnes, J. F. Hutton, and K. Walters, *An Introduction to Rheology* (Elsevier, Amsterdam, 1989).
[3] B. D. Todd and P. J. Daivis, Mol. Simul. **33**, 189 (2007).
[4] C. N. Likos, Phys. Rep. **348**, 267 (2001).
[5] P. Mausbach and H.-O. May, Fluid Phase Equilib. **249**, 17 (2006).
[6] P. Mausbach and H.-O. May, Z. Phys. Chem. **223**, 1035 (2009).
[7] H.-O. May and P. Mausbach, Phys. Rev. E **76**, 031201 (2007).
[8] W. P. Krekelberg, T. Kumar, J. Mittal, J. R. Errington, and T. M. Truskett, Phys. Rev. E **79**, 031203 (2009).
[9] O. Pizio, H. Dominguez, Y. Duda, and S. Sokolowski, J. Chem. Phys. **130**, 174504 (2009).
[10] A. Lang, C. N. Likos, M. Watzlawek, and H. Löwen, J. Phys.: Condens. Matter **12**, 5087 (2000).
[11] A. A. Louis, P. G. Bolhuis, J. P. Hansen, and E. J. Meijer, Phys. Rev. Lett. **85**, 2522 (2000).
[12] S. A. Baeurle and J. Kroener, J. Math. Chem. **36**, 409 (2004).
[13] D. J. Evans and G. P. Morriss, *Statistical Mechanics of Nonequilibrium Liquids*, 2nd ed. (Academic, London, 2008).

[14] J. Ge, G.-W. Wu, B. D. Todd, and R. J. Sadus, J. Chem. Phys. **119**, 11017 (2003).
[15] D. J. Evans, W. G. Hoover, B. H. Failor, B. Moran, and A. J. C. Ladd, Phys. Rev. A **28**, 1016 (1983).
[16] R. J. Sadus, *Molecular Simulation of Fluids: Theory, Algorithms, and Object-Orientation* (Elsevier, Amsterdam, 1999).
[17] C. W. Gear, *Numerical Initial Value Problems in Ordinary Differential Equations* (Prentice-Hall, Englewood Cliffs, NJ, 1971).
[18] P. Mausbach, A. Ahmed, and R. J. Sadus, J. Chem. Phys. **131**, 184507 (2009).
[19] J. J. Erpenbeck, Phys. Rev. Lett. **52**, 1333 (1984).
[20] L. V. Woodcock, Phys. Rev. Lett. **54**, 1513 (1985).
[21] D. J. Evans and G. P. Morriss, Phys. Rev. Lett. **56**, 2172 (1986).
[22] J. Delhommelle, Phys. Rev. E **71**, 016705 (2005).
[23] J. Delhommelle, J. Petravic, and D. J. Evans, Phys. Rev. E **68**, 031201 (2003).
[24] G. C. Kalur, B. D. Frounfelker, B. H. Cipriano, A. I. Norman, and S. R. Raghavan, Langmuir **21**, 10998 (2005).
[25] J. T. Bosko, B. D. Todd, and R. J. Sadus, J. Chem. Phys. **121**, 12050 (2004).
[26] J. Ge, B. D. Todd, G. Wu, and R. J. Sadus, Phys. Rev. E **67**, 061201 (2003).
[27] K. P. Travis, D. J. Searles, and D. J. Evans, Mol. Phys. **95**, 195 (1998).
[28] C. Trozzi and G. Ciccotti, Phys. Rev. A **29**, 916 (1984).
[29] M. M. Cross, J. Colloid Sci. **20**, 417 (1965).
[30] B. D. Todd, Phys. Rev. E **72**, 041204 (2005).